This is a repository copy of *Design and analysis of novel asymmetric-stator-pole flux reversal PM machine*.

Design and Analysis of Novel Asymmetric-Stator-Pole Flux Reversal PM Machine

Abstract—This paper proposes a novel flux reversal permanent magnet (FRPM) machine with asymmetric-stator-pole (ASP) configuration. Different from the conventional FRPM machine with uniform "NS-NS-NS" PM sequence, the proposed ASP-FRPM machine is characterized by a "NSN-S-NSN" magnet arrangement. Hence, the interpolar flux leakage is significantly reduced with the developed design, which can improve the torque capability. The machine topologies, features and operating principle are introduced, respectively. A simplified magnetic circuit model is established to reveal the underlying flux leakage reduction mechanism of the ASP design, and the rotor pole number is analytically optimized as well. The design parameters are then globally optimized so as to improve the torque quality. In addition, the electromagnetic characteristics of the ASP- and conventional FRPM machines are compared. Finally, experiments have been carried out to validate the theoretical results.

Index Terms—Asymmetric stator pole, flux leakage, flux reversal, permanent magnet (PM) machine, reluctance machine.

I. INTRODUCTION

DUE to the distinct feature that neither permanent magnets (PMs) nor windings are located on the rotor, the stator PM machines [1] have been of increasing research interest in the last decade, which are recognized as promising candidates for aircraft and traction applications. Apart from inheriting simple salient rotor structure of switched reluctance machines (SRMs) [2]-[4], the merits of easy thermal management, as well as high torque density can be achieved with the stator PM machines. More importantly, the stator PM machines can behave in a similar way as either brushless DC or AC PM synchronous machines [3] [4].

Compared to the other three kinds of stator PM machine, i.e., doubly salient [5] [6] , stator slot [7], and switched flux PM machines [8] [9], flux reversal PM (FRPM) machines can offer the advantages of good torque density and high magnet utilization ratio [10]-[26]. Meanwhile, their stator/rotor laminations are geometrically similar to those of SRMs [2]-[4], which results in structural simplicity, strong robustness, and ease of manufacturing. Therefore, FRPM machines are suitable for low-speed direct-drive systems [10] and high-speed applications [11], such as electric vehicle [11] and wind power generation, etc. [12]. In fact, FRPM machines are of growing research interests in the last decade [10]-[26]. In terms of winding configuration, the feasibilities of the fractional-slot concentrated [13] and full-pitch distributed [14] windings for the FRPM machines are investigated, respectively. It shows that their torque density can be improved with appropriate stator-slot/rotor-pole combinations [13]. For PM arrangements, it is reported that the FRPM machines having more than two PMs per stator pole may exhibit higher torque density [15], which are proved to be competitive candidates for low-speed high-torque applications. In addition, Halbach [16] and consequent-pole PM configurations [17]-[19] are employed to improve the torque capability with reduced magnet usage. The FRPM machines with even uniform PM arrays [20] are presented to perform the torque enhancement effect well. The FRPM machines with different magnet arrangements are summarized and compared in [21], which is helpful for providing a valuable design guidance. From the perspective of the working principle, FRPM machine can be regarded as a magnetic gear (MG), where stationary PM magnetic fields are modulated by salient rotor poles [22] [23]. It reveals that all PM magneto-motive-forces (MMFs) and only fundamental permeance are engaged in the torque production [23]. Nevertheless, the conventional FRPM machines [10]-[26] generally suffer from serious PM flux leakage, resulting in restricted torque capability. This is recognized as a major challenging issue for the existing FRPM machines.

To date, many efforts have been made in order to reduce the flux leakage [24]-[26]. Apart from the abovementioned alternate PM arrangement [16] [17], the stator and rotor tooth notching are the main countermeasures in literature [24]-[26]. However, the flux leakage reduction effect due to the stator/rotor slotting is unobvious. Therefore, this paper proposes a novel asymmetric-stator-pole (ASP) FRPM (ASP-FRPM) machine, which can effectively reduce the flux leakage and improve the torque capability. Different from the conventional FRPM machine with uniform "NS-NS-NS" PM sequence, the proposed ASP-FRPM machine is geometrically characterized by a "NSN-S-NSN" magnet arrangement.

This paper will be organized as follows. In Section II, the ASP-FRPM topology, features and working principle are introduced, respectively. Then, a simplified analytical model is implemented to reveal the underlying flux leakage suppression effect of the ASP design in Section III. In Section IV, the rotor pole number is analytically optimized, and the geometric parameters are globally optimized to improve the torque quality. Besides, Section V is devoted to the performance comparison between the ASP-FRM and its conventional FRPM machine counterpart. Finally, the theoretical results are experimentally validated in Section VI, followed by conclusion in Section VII.

II. TOPOLOGIES, FEATURES AND WORKING PRINCIPLE

A. FRPM Machine Topologies

The topologies of 12-stator-slot/17-rotor-pole conventional FRPM and ASP-FRPM machines are shown in Figs. 1(a) and (b), respectively. The major difference between these two machines lies in the magnet arrangement. Each stator pole of the conventional one carries two pieces of PMs with alternating polarities, i.e., "NS-NS-NS-…"[10]-[15], [20]-[26], while the ASP design features asymmetric magnet configuration, i.e., "NSN-S-NSN…". It should be noted that the number of total PM pieces and magnet usages of the two machines are identical. For the two FRPM machines, the single-layer non-overlapping armature windings are wound on the stator teeth having three PM segments.
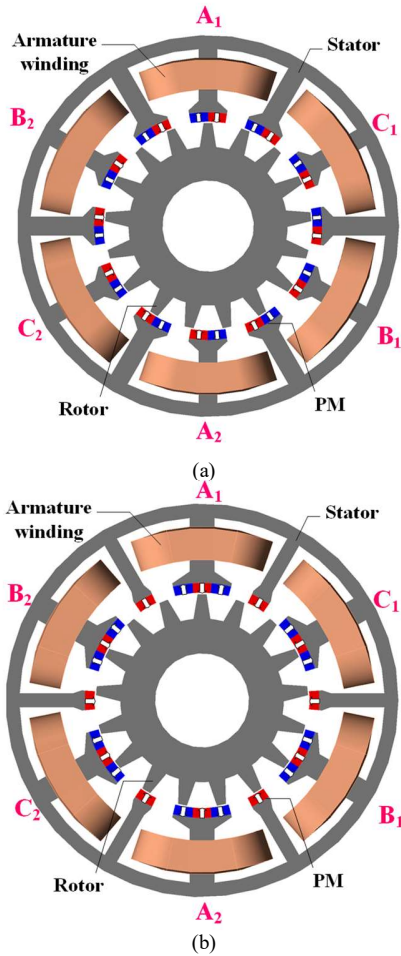

(a)

(b)

Fig. 1. Topology of 12/17-pole FRPM machines. (a) Conventional. (b) ASP.

B. Working Principle

Similar to the conventional stator PM machines [8], the working principle of the proposed ASP-FRPM machine is based on the variable reluctance behavior, namely, the alignment and misalignment between the doubly salient stator and rotor poles produce the basically sinusoidal coil flux linkage, as shown in Fig. 2. The open-circuit field distributions corresponding to four typical rotor positions are plotted in Fig. 3. It shows that although the coil flux linkage is unipolar, the resultant phase flux linkage turns out to be bipolar due to the

cancellation of the DC bias and even-order harmonics in the coil flux linkage. In order to obtain symmetrical and bipolar phase flux linkage, the stator-slot/rotor-pole numbers N_s and N_r should satisfy [8]

$$\frac{N_s}{GCD(N_s, N_r)} = 2k, \; k = 0,1,2,... \tag{1}$$

where GCD denotes the greatest common divisor.
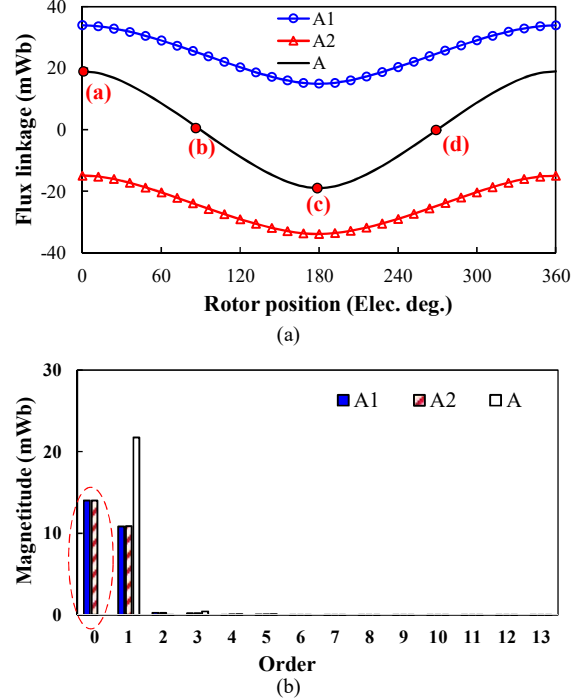

(a)

(b)

Fig. 2. Flux linkage characteristics of proposed 12/17-pole ASP-FRPM machine. (a) Coil and phase-A flux linkage. (c) Harmonic spectra.
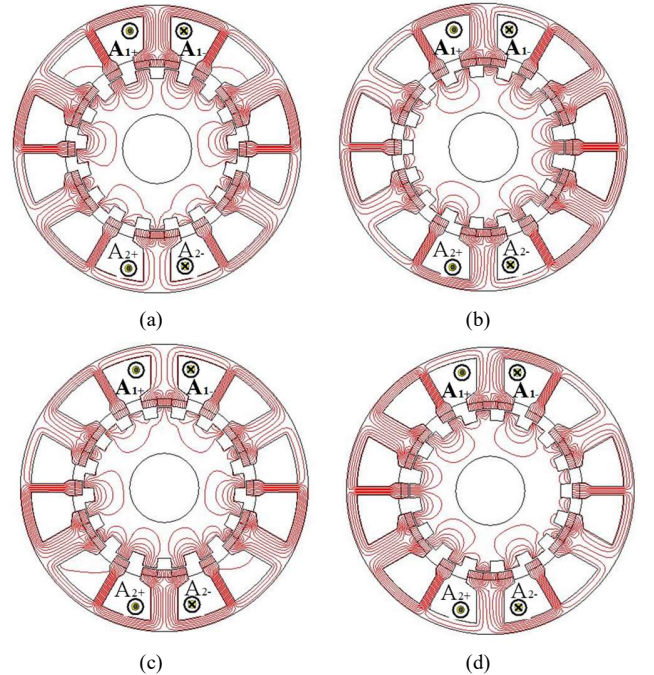

Fig. 3. Operating principle of 12/17-pole ASP-FRPM machine. (a) θ_e=0°. (b) θ_e=90°. (c) θ_e=180°. (d) θ_e=270°.

III. INVESTIGATION OF FLUX LEAKAGE REDUCTION MECHANISM

In order to provide insightful understanding for the flux leakage reduction mechanism of the proposed ASP-FRPM machine, a magnetic circuit based method coupled with the air-gap permeance model [8] is employed.

First, we analyze the flux leakages of conventional and ASP-FRPM machines by using the ideal slotless models as shown in Fig. 4. Obviously, based on the simplified magnetic circuit models, the interpole flux leakage $\Phi_{\delta 1}$ per stator pole of the conventional FRPM machine can be expressed as

$$\Phi_{\delta 1} = \frac{2F_m}{2R_m + 2R_g} = \frac{F_m}{R_m + R_g} \quad (2)$$

where F_m and R_m denote the magneto-motive-force and magnetic reluctance of one PM segment, and R_g is the air-gap magnetic reluctance under one PM pole. It should be noted that the iron magnetic reluctance is ignored in this case due to the relatively short leakage path. Hence, the total flux leakage of all the stator poles $\Phi_{\delta s1}$ are yielded as

$$\Phi_{\delta s1} = 12\Phi_{\delta 1} = \frac{12F_m}{R_m + R_g} \quad (3)$$

Since there is barely effective flux linking coil A_1 for the slotless model of the conventional FRPM machine, the coil flux linkage turns out to be bipolar with the modulation of the rotor salience.
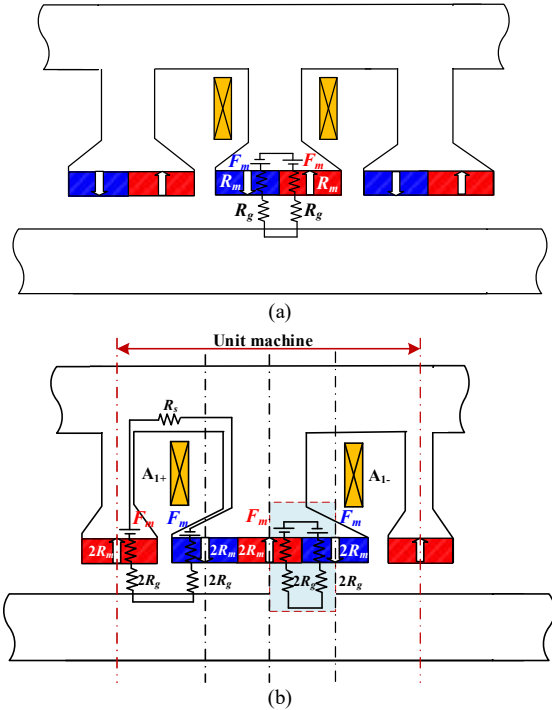

(a)

(b)

Fig. 4. Slotless models of (a) conventional and (b) ASP-FRPM machines.

On the other hand, due to the symmetry, one unit of the slotless model of ASP-FRPM machine is taken as an example as illustrated in Fig. 4(b). The unit machine can be subdivided into 4 portions. Due to the symmetry, the middle two portions suffer from the interpole flux leakage, while the sided two portions produces "effective" flux. Consequently, the interpole flux leakage $\Phi_{\delta 2}$ in one wound stator pole can be represented by

$$\Phi_{\delta 2} = 2 \times \frac{2F_m}{2R_m + 2R_m + 2R_g + 2R_g} = \frac{F_m}{R_m + R_g} \quad (4)$$

Thus, for the ASP-FRPM machine, the entire flux leakage of all the stator poles $\Phi_{\delta s2}$ are

$$\Phi_{\delta s2} = 6\Phi_{\delta 1} = \frac{6F_m}{R_m + R_g} \quad (5)$$

From (2) and (5), it can be derived that the overall flux leakage of the ASP-FRPM machine is half of that of the conventional counterpart. That is to say, the flux leakage reduction effect of the ASP design is analytically identified. Moreover, its effective per wound stator pole can be expressed as

$$\Phi_{m2} = 2 \times \frac{2F_m}{2R_m + 2R_m + 2R_g + 2R_g + R_s} = \frac{F_m}{R_m + R_g + \frac{R_s}{4}} \quad (6)$$

where R_s is the magnetic reluctance of the stator iron part. Hence, this biased flux Φ_{m2} in the proposed ASP design results in the torque improvement when the air-gap field modulation works due to the rotor salient poles. It should be noted that the abovementioned analyses are employed to simply quantitatively confirm that the proposed AS-FRPM machine show less overall PM flux leakage than the conventional one. In order to confirm the rationality of the theoretical analyses, the open-circuit field distributions of the two FRPM machines are shown in Fig. 5. Apparently, the conventional FRPM machine shows more significant flux leakage than the proposed ASP-FRPM machine, as evidenced by the flux density distributions on the stator yoke.

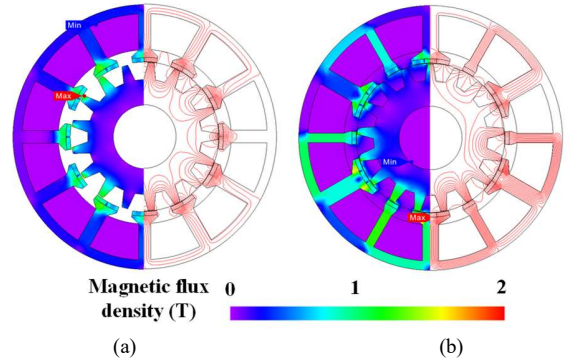| Magnetic flux density (T) | 0 | 1 | 2 |

(a)   (b)

Fig. 5. Open-circuit field distribution plots of the two 12/17-pole FRPM machines. (a) Conventional. (b) ASP.
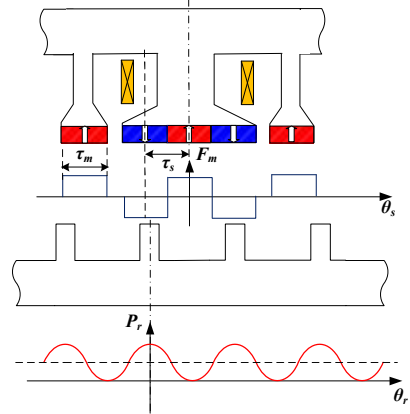

Fig. 6. Simplified permeance model of ASP-FRPM machine.

IV. DESIGN OPTIMIZATION APPROACH

A. Analytical Optimization of Rotor Pole Number

Similar to other conventional FRPM machines [15] [22] [23], the proposed ASP-FRPM machine can be considered as a flux-modulation machine working based on "magnetic-gearing (MG) effect". The simplified analytical models of the ASP-FRPM machines accounting for the rotor slotting, are illustrated in Fig. 6. The stationary PM fields are modulated by the rotating iron poles, yielding abundant air-gap field harmonics which engage in the torque production.

First, the excitation MMF distribution F_m can be expressed as its Fourier series expansion

$$F_m = \sum_i F_{mi} \cos(iN_s\theta_s) \qquad (7)$$

where N_s is the stator slot number, θ_s is the relative angular position of the stator, and F_{mi} denotes the PM MMFs, which can be expressed as

$$F_{mi} = \frac{2B_{rm}h_{pm}}{i\pi\mu_0\mu_r} \left\{ \begin{array}{c} -\sin\left(\frac{1}{2}i\pi\beta\right) + \sin\left(i\pi\frac{3}{2}\beta\right) \\ -\sin\left(i\pi\frac{1}{2}\beta\right) + \sin\left[i\pi\left(1-\frac{\beta}{2}\right)\right] \end{array} \right\} \quad (8)$$

where B_{rm} is the remanence flux density of PM, h_{pm} is the PM thickness, β is the pole-arc ratio, which denotes the ratio of the PM arc angle to the stator arc angle per pole. Besides, the air-gap permeance $\Lambda_r(\theta_s, \theta_r)$ due to the rotor slotting can be given by ignoring the high-order harmonics, i.e. [26]

$$\Lambda_r(\theta_s, \theta_r) = \frac{\mu_0}{g + \delta(\theta_s, \theta_r)} = \Lambda_{r0} + \sum_{j=1}^{\infty} \Lambda_{rj}\cos\left[jN_r(\theta_s - \theta_r)\right] \quad (9)$$

where N_r is the rotor pole number, θ_r is the relative angular positions of the rotor, and the equivalent air-gap length $\delta(\theta_s, \theta_r)$ can be represented by

$$\delta(\theta_s, \theta_r) = a_0 + \left\{ \sum_{n=1}^{\infty} a_n\cos\left[nN_s(\theta_s - \theta_r)\right] + b_n\sin\left[nN_s(\theta_s - \theta_r)\right] \right\} \quad (10)$$

where the coefficients a_0, a_n and b_n are expressed as

$$a_0 = \frac{R_{ro}(\pi\beta_r)^2}{6N_r} \quad (11)$$

$$a_n = -\frac{R_{ro}}{2N_r n^2}\left[(1+\cos(2\pi\beta_r)) - \frac{1}{\pi n\beta_s}\sin(2\pi n\beta_r)\right] \quad (12)$$

$$b_n = \frac{R_{ro}}{2N_r n^2}\left[\frac{1}{\pi n\beta_r}(1-\cos(2\pi\beta_r)) - \sin(2\pi n\beta_r)\right] \quad (13)$$

where β_s denotes the rotor slot opening ratio, R_{ro} is the rotor outer radius. The resultant air-gap flux density $B_r(\theta_s, \theta_r)$ can be obtained as

$$\begin{aligned} B(\theta_s, \theta_r) &= F_{PM}(\theta_s, \theta_r)\Lambda_r(\theta_s, \theta_r) \\ &= \frac{1}{2}\sum_{i=1,2,3...}^{\infty}\sum_{j=0,1,2...}^{\infty} F_i\Lambda_{rj}\cos[(i\frac{N_s}{2}\pm jN_r)\theta_s \mp jN_r\theta_r] \end{aligned} \quad (14)$$

The flux linkage of coil A$_1$ can be further expressed as [23]

$$\begin{aligned} \psi_{A1} &= N_c\int B(\theta_s, \theta_r)d\theta_s \\ &= \sum_{i=1,2,3...}^{\infty}\sum_{j=0,1,2...}^{\infty} \frac{F_i\Lambda_{rj}N_cL_{stk}R_{si}}{i\frac{N_s}{2}\pm jN_r}\sin[(i\frac{N_s}{2}\pm jN_r)\frac{2\pi}{N_s}]\cos[\mp jN_r\theta_r] \end{aligned} \quad (15)$$

where N_c is the number of turns per coil, L_{stk} is the effective stack length, R_{si} is the stator inner radius. Since the two coils A$_1$ and A$_2$ are with 180 electrical degrees phase shifting, the flux linkage of coil A$_2$ can be analogously given by

$$\psi_{A2} = \sum_{j=0,1,2...}^{\infty} \frac{F_i\Lambda_jN_cL_{stk}R_{si}}{i\frac{N_s}{2}\pm jN_r}\sin[(i\frac{N_s}{2}\pm jN_r)\frac{2\pi}{N_s}]\cos[(i\frac{N_s}{2}\pm jN_r)\pi \mp jN_r\theta_r] \quad (16)$$

As a result, the open-circuit phase flux linkage Ψ_m is given by synthesizing the flux linkages of two oppositely connected coils A$_1$ and A$_2$

$$\psi_m = \psi_{A1} + \psi_{A2} \quad (17)$$

Due to its negligible reluctance torque, the torque equation of the proposed ASP-FRPM machine can be expressed as

$$T_e = \frac{3}{2}N_r\Psi_mI_q \quad (18)$$

where T_e denotes the average electromagnetic torque, and I_q is the q-axis current.

The analytically predicted torques under different rotor pole number are compared with the FE results in Fig. 7. It shows that the 12-stator-slot/17-rotor-pole ASP-FRPM machine has the highest torque capability, which is selected for the following investigation.
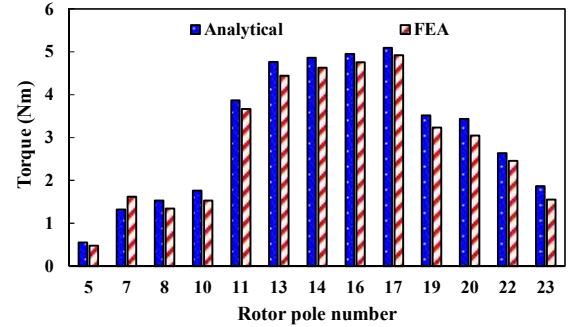

Fig. 7. FE and analytical predicted torques under different rotor pole number.

B. Parametric Optimization

The multi-objective genetic algorithm (GA) embedded in JMAG 15.1 software package is employed to optimize the torque quality with the constraints of the overall dimensions, the slot packing factor of 0.5, and the rated current density of 5A/mm^2. The geometric parameters are defined in Fig. 8, and their corresponding scopes are listed in Table I. all the design variables are globally optimized with multi-objective genetic algorithm [28]-[30], which can be employed to achieve an optimum design without considering the optimization sequence. Meanwhile, the constraint ranges are assigned in order to avoid the conflicts and errors during the geometric modeling process. optimization goal is to simultaneously maximize the average torque (T_{ave}) and minimize the torque ripple (T_{rip}), of which the weight factors are 1.0 and 0.5, respectively. The settings of GA are as follows: the population size, mating pool size, individual crossover probability and mutation probability are 20, 20, 0.5 and 1, respectively.
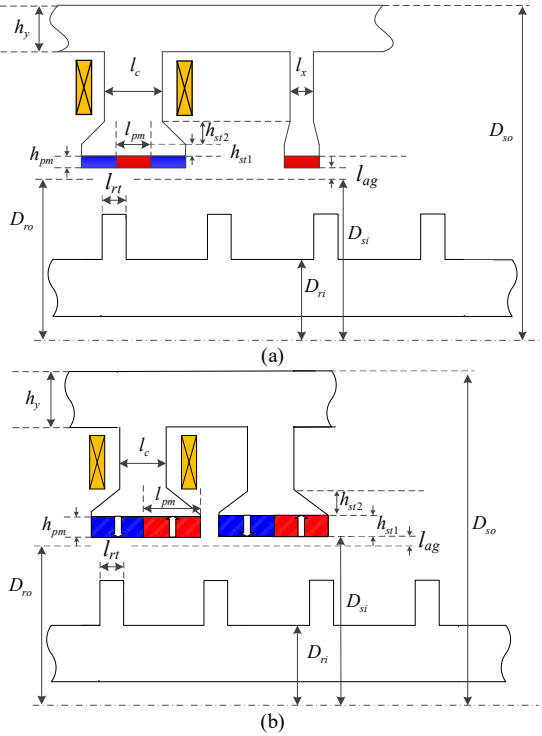
Fig. 8. Illustration of design parameters of (a) ASP- and (b) conventional FRPM machines.

TABLE I
RANGE OF DESIGN PARAMETERS OF 12/17-POLE ASP- AND CONVENTIONAL FRPM MACHINE

Parameters	Range
Stator inner diameter D_{si}	50~70mm
Wound stator tooth width l_c	2~12 mm
Unwound stator tooth width l_x	2~12 mm
PM width l_{pm}	5~14 degrees
PM thickness h_{pm}	0.5~5 mm
Stator tooth tip height h_{st1}	0.5~4 mm
Stator back iron h_y	0.5~5 mm
Rotor pole height h_{rt}	2~7 mm
Rotor tooth width l_{rt}	1~10 degrees

Fig. 9 shows the optimization results of the proposed ASP- and conventional FRPM machines, the case with "$T_{ave} \approx 6.65$Nm" and "$T_{rip} \approx 3.5\%$" are selected for the ASP case, while "$T_{ave} \approx 5.34$Nm" and "$T_{rip} \approx 2.4\%$" are chosen for the conventional case in the following investigation. This can well balance the trade-off between the torque capability and the torque ripple.

C. Influences of Selected Design Parameters

Based on the globally optimized design as a benchmark, only parts of design parameters that are identified as dominant ones reported in previous relevant literatures [28]-[30] are selected. Then, the influences of those selected parameters on the torque capability are evaluated in order to reveal some useful design guidelines for the ASP-FRPM machine [12].

a) Split Ratio

The split ratio is defined as the ratio of the inner stator diameter to the outer stator diameter. Fig. 10(a) shows the variation of the average torque with the split ratio. It shows that for the two cases, the torque rises first, and then drops steadily when the split ratio exceeds 0.6. This is mainly attributed to the

fact that the PM area are enlarged with the increase of the split ratio. However, as the split ratio is higher than the optimal value, the reduced stator slot area with increasing spilt ratio results in the torque decrease in turn.
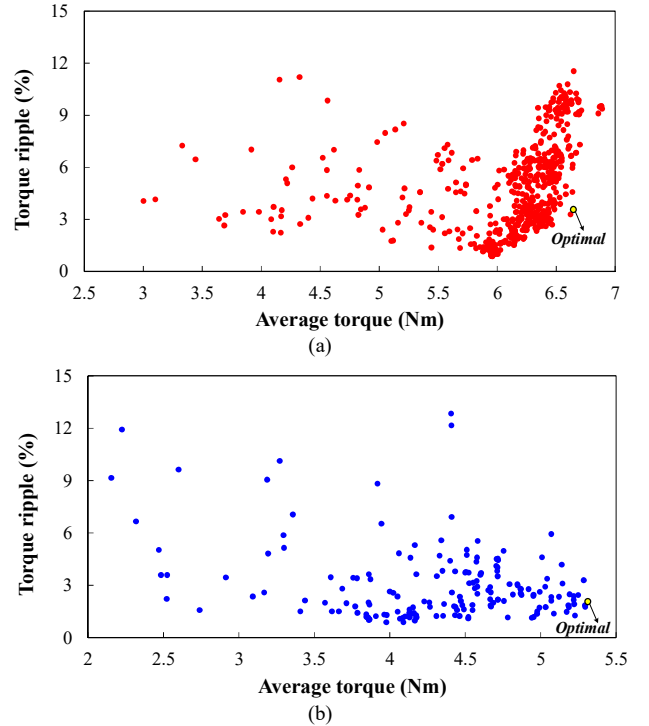

Fig. 9. Optimization results of 12/17-pole (a) ASP- and (b) conventional FRPM machines.

b) Stator/Rotor Slot Opening Ratios

The stator/rotor slot opening ratios are defined as the slot openings to the stator/rotor pole pitch. Fig. 10(b) shows the torque as a function of the slot opening ratio. It can be observed that the optimal stator/rotor slot opening ratios are 0.33 and 0.45 for the proposed ASP case, while 0.23 and 0.35 for the conventional case. This phenomenon is due to the fact that the decrease of the stator slot opening ratio leads to the PM area enlargement, while the flux leakage tends to be serious when the ratio is lower than the optimal value. Similar trends can be observed in the "rotor slot opening ratio" case as well. Higher rotor slot opening ratio increases the effective PM flux penetrating into the rotor iron part, whereas significant PM flux leakage happens as the ratio exceeds the optimal value.

c) Stator tooth width

A stator width ratio is defined as the ratio of the wound stator tooth width to the unwound one in order to investigate the relation between two widths. The variations of the average torques with the stator width ratio under various l_c are plotted in Fig. 10(c), it shows that the optimum stator ratio decreases with higher wound stator tooth width. As a result, it is necessary to optimize the two stator widths simultaneously, which are both considered in the global optimization without mutual restriction.

The influences of the wound and unwound stator teeth widths on the torque capability are illustrated in Figs. 10(e) and (f), respectively. For the proposed ASP-/conventional FRPM

machine, the optimal values are 6.26mm/4.80mm and 3.50mm/4.80mm for the wound and unwound stator teeth, respectively.

d) PM Thickness

Fig. 10(f) shows the torque variation with the PM thickness. It demonstrates that the torque rises with increasing the PM thickness first due to the increase of the effect PM flux, while then drops dramatically caused by the increase of the effective air-gap length. In order to prevent the unexpected PM demagnetization risk induced by the short-circuit fault and the overloading operation, the PM thickness is usually selected as 4~6 times the air-gap length, i.e., 2.4mm for the machine manufacturing [20].
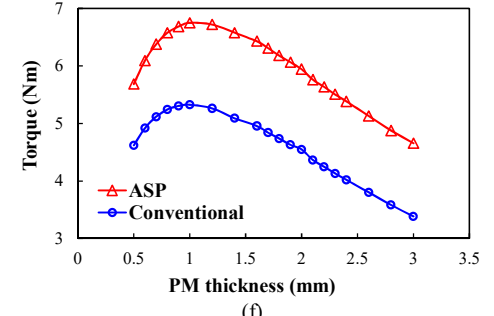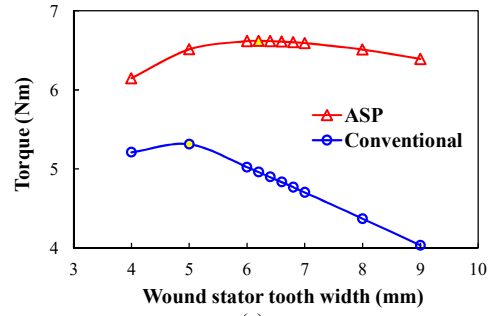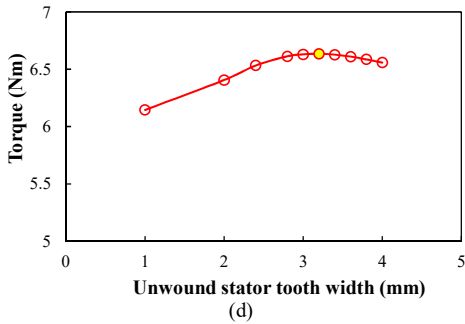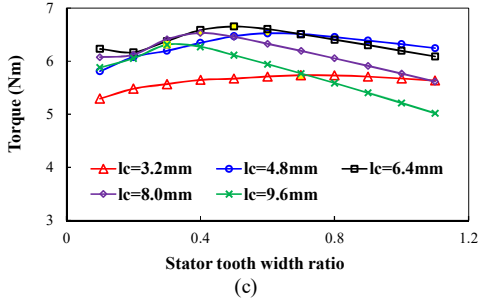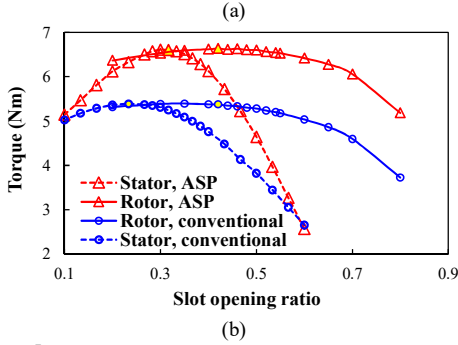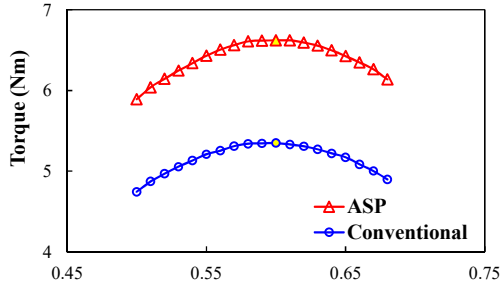

Fig. 10. Effects of design parameters on the torque capability. (a) Split ratio. (b) Stator/rotor slot opening ratios. (c) The variations of the average torques with the stator width ratio under various l_c. (d) Unwound stator tooth width. (e) Wound stator tooth width. (f) PM thickness.
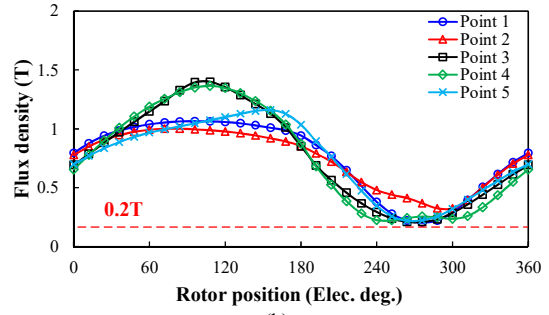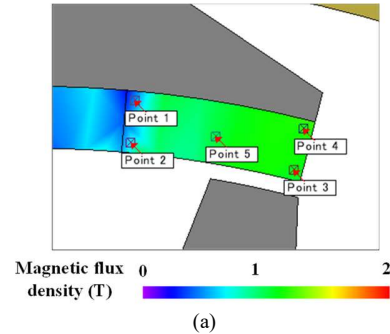
Fig. 11. (a) Field distributions and (b) PM operating points of the proposed ASP-FRPM machine under 2.5 times overload, and temperature=120°C.

D. Demagnetization Examination

In order to confirm the feasibility of the previously designed PM thickness, the demagnetization withstand capability of the ASP-FRPM machine is examined. Fig. 11 shows the working point variations of five typical PM points under 2.5 times overload operation, and the PM material and the temperature are set as N35SH and 120°C, respectively. The reference knee flux density is approximately 0.2T. The lowest operating point

is approximately 0.22T, which exceeds the threshold value. This indicates that the local demagnetization can be well eliminated with the optimized design.

V. ELECTROMAGNETIC PERFORMANCE COMPARISON

In order to confirm the feasibility and advantages of the proposed ASP-FRPM machine design, its electromagnetic characteristics are compared with those of the conventional FRPM machine. For fair comparison, both FRPM machines have been globally optimized, which share identical stator-slot/rotor-pole numbers (12/17), winding configuration, overall PM polarity sequence, and magnet usage, etc. The major design parameters of two investigated machines are listed in Table II.

TABLE II
MAJOR DESIGN PARAMETERS OF 12/17-POLE FRPM MACHINES WITH CONVENTIONAL AND ASP CONFIGURATIONS

Machine types	Unit	Conventional	ASP
Rated speed	r/min	1000	
Rated current	Arms	10	
Stator outer diameter	mm	100	
Air-gap length	mm	0.4	
Active stack length	mm	80	
Split ratio	-	0.6	
Stator back-iron thickness	mm	3.5	
Wound stator tooth width	mm	4.80	6.26
Unwound stator tooth width	mm	4.80	3.25
Stator inner diameter	mm	60.5	59.8
Rotor pole height	mm	5	
Stator slot opening ratio	-	0.23	0.33
Rotor slot opening ratio	-	0.35	0.45
Air-gap length	mm	0.4	
NdFeB magnet thickness	mm	2.4	
PM width	deg.	19	
Magnet grade	-	N35SH	
Steel grade	-	35CS300	

A. Open-Circuit Performance

The open-circuit air-gap flux density and back-EMF waveforms of the ASP- and conventional FRPM machines, as well as the regular SPM machine with same winding configuration and rotor pole numbers are shown in Figs. 12 and 13, respectively. It shows that the ASP machine exhibits more working harmonics, and hence much higher fundamental EMF magnitude than its conventional counterpart. This is mainly due to the flux leakage reduction effect of the proposed ASP design, as mentioned in Section III. In addition, the back-EMF magnitude of the SPM machine is slightly lower than that of the conventional FRPM machine. This is mainly attributed to more pronounced flux modulation effect (see Fig. 12(b)) of the FRPM machine despite their lower main air-gap flux harmonics (6th, 12nd, 18th, etc.) than that of the regular SPM machine, which are stationary and non-working.

B. Torque Characteristics

The torque characteristics of the two FRPM machines are investigated and compared as shown in Fig. 14. The cogging torque waveforms are shown in Fig. 14(a). It can be seen that the peak cogging torque of the conventional FRPM machine is slightly lower than that of the proposed ASP one, which is mainly attributed to the existence of more abundant air-gap field harmonics of the ASP case, as evidenced in Fig. 12(b). In order to confirm the suitable control strategy to maximize the

torque capability, the torque-current angle characteristics are analyzed in advance, as shown in Fig. 14(b). It is obvious that both two FRPM machines show a unity saliency ratio. In addition, the steady-state torque waveforms of FRPM machines under both rated current (I_{rms}=10A, "rms" denotes root-mean-square value) and zero d-axis current (I_d) control are shown in Fig. 14(c). It demonstrates that the ASP-FRPM machine provides 24.16% higher average torque, together with 30% lower torque ripple than its conventional counterpart. This is mainly due to the flux leakage reduction. Fig. 14(d) shows the torque versus current characteristics of the two machines, which indicates that the proposed ASP design has better torque capability. However, the proposed ASP-FRPM machine exhibits non-linear torque-current characteristics due to the magnetic saturation caused by the biased flux linkage.
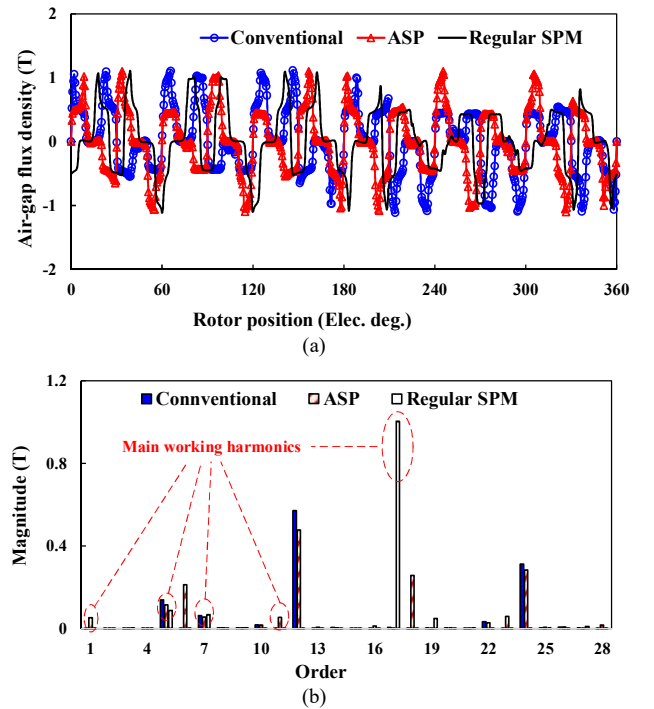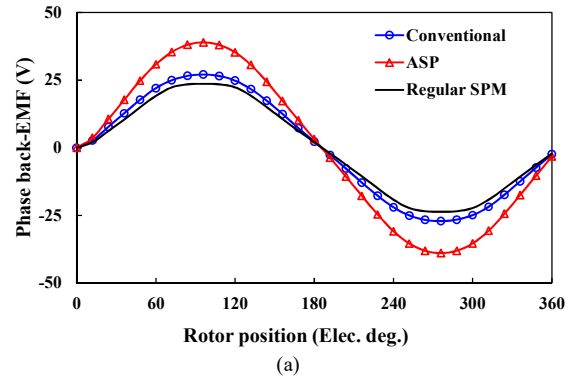

Fig. 12. Open-circuit air-gap flux density waveforms of the two 12/17-pole FRPM machines and regular SPM machine. (a) Waveforms. (b) Harmonic spectra.
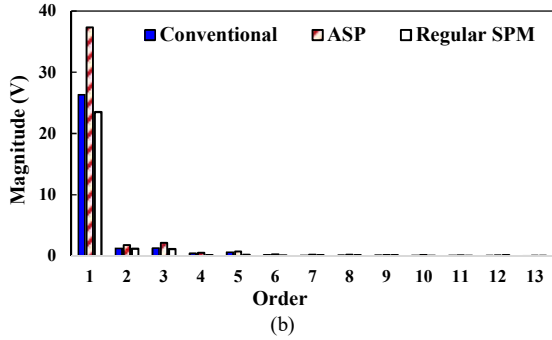

(a)

(b)

Fig. 13. Phase back-EMFs of the two 12/17-pole FRPM machines and regular SPM machine, 1000r/min. (a) Waveforms. (b) Harmonic spectra.
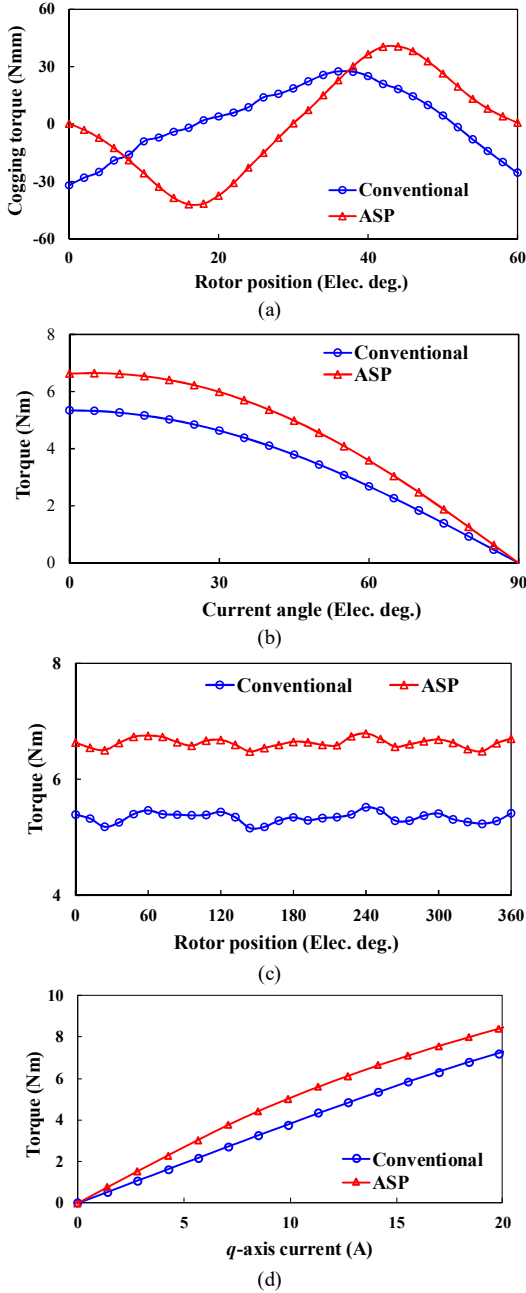

(a)

(b)

(c)

(d)

Fig. 14. Torque characteristics of the conventional and ASP-FRPM machines. (a) Cogging torque. (b) Torque vs current angle. (c) Steady-state torque. (d) Torque vs q-axis current.

C. Power Factor

The power factor PF can be calculated by the phasor diagram under $I_d=0$ control as shown in Fig. 15, i.e., [20]

$$PF = \cos\theta = \frac{1}{\sqrt{1+(\omega_e L_s I_s / E_0)^2}} = \frac{1}{\sqrt{1+(L_s I_s / \psi_m)^2}} \qquad (19)$$

where I_s is the stator current, L_s is the synchronous inductance, ω_e is the electrical angular speed, E_0 is the open-circuit back-EMF fundamental magnitude, U is the terminal voltage, and θ is the angle difference between E_0 and U. The resultant inductance, phase flux linkage and power factor are listed in Table III. It shows that the proposed ASP-FRPM machine exhibits a 29% higher power factor than the conventional FRPM machine. This is mainly attributed to higher EMF and lower inductance of the proposed ASP design.
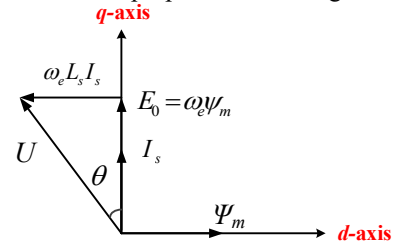

Fig. 15. Phasor diagram of the FRPM machines under $I_d=0$ control.

TABLE III
INDUCTANCE, PHASE FLUX LINKAGE, POWER FACTORS OF 12/17-POLE FRPM MACHINES WITH CONVENTIONAL AND ASP CONFIGURATIONS

Items	Unit	Conventional	ASP
Synchronous inductance	mH	1.91	1.61
Phase flux linkage	mWb	14.95	21.13
Power factor	-	0.62	0.80

D. Loss and Efficiency Evaluation

Fig. 16 shows the iron loss characteristics of the two FRPM machines. Fig. 16(a) demonstrates that the ASP machine shows slightly higher hysteresis and eddy-current losses than the conventional counterpart. This is mainly due to more magnetic saturation in the stator core of the ASP-FRPM machine caused by its flux leakage reduction, as clearly illustrated in Fig. 16(b). In addition, the PM loss against speed curves with or without PM axial segmentations are shown in Fig. 17, it can be seen that the PM eddy-current losses account for 11.7% and 16.3% of the total loss for the conventional and ASP structures, respectively. Consequently, 4-division PM axial segmentation is employed for the prototype manufacturing, which can reduce the PM loss by approximately 2/3. Moreover, the efficiency versus speed characteristics are plotted in Fig. 18. Overall, the iron loss components, the magnet loss, the copper loss and the efficiency at the rated load and speed are listed in Table IV. Due to higher torque capability, the ASP machine exhibits higher efficiency than its conventional counterpart albeit with higher iron loss PM eddy-current loss, and comparable copper loss.
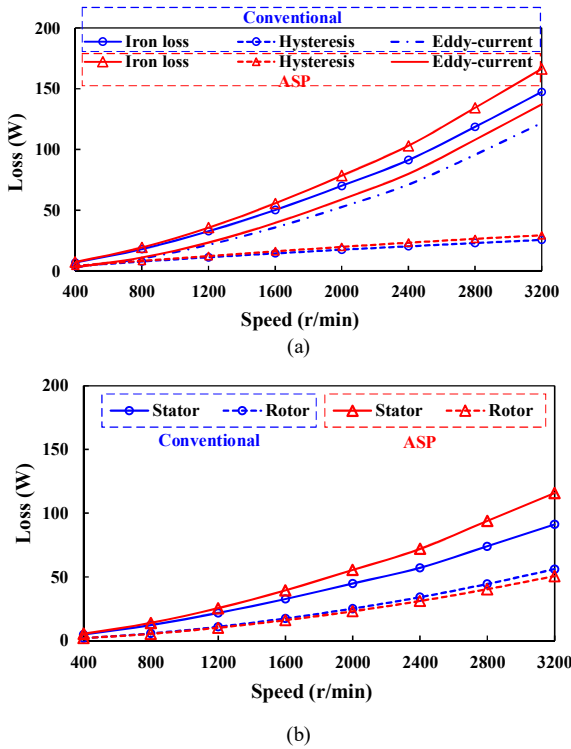
Fig. 16. Iron loss characteristics of the conventional and ASP-FRPM machines. (a) Iron loss versus speed curves. (b) Stator and rotor iron loss components versus speed curves.
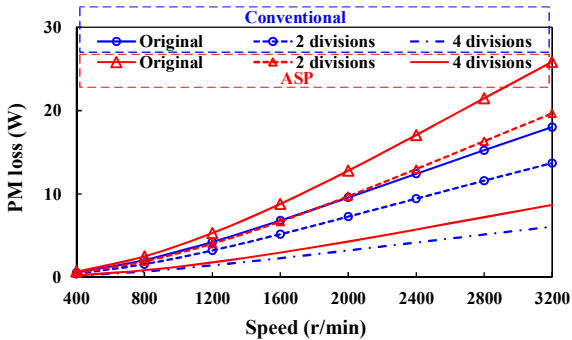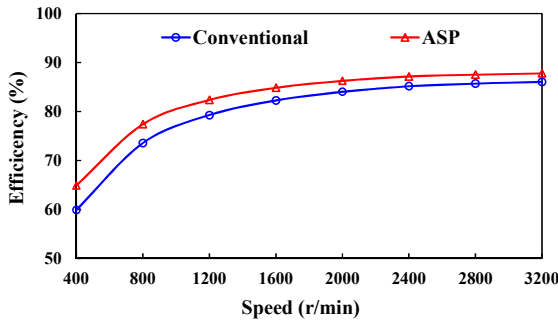

Fig. 17. PM loss subject to axial PM segmentations.

Fig. 18. Efficiency versus speed curves at rated load.

E. Torque-Speed Curves

The flux-weakening performance of the two machines is evaluated. First, a flux-weakening factor k_{fw} that characterizes the capability extending the speed range above the base speed can be defined as [27]

$$k_{fw} = \frac{L_d i_{\lim}}{\Psi_m} \quad (19)$$

where i_{lim} and L_d are the maximum phase current and the d-axis inductance; As a result, the base speed, peak power, and k_{fw} etc. are listed in Table V. The torque/power-speed curves of the two FRPM machines are shown in Fig. 19. It can be seen that both machines can achieve theoretically infinite constant-power speed range for the given inverter power rating since the flux-weakening coefficients are higher than 1. The base speed of the conventional case is slightly higher than that of the ASP one, which is mainly attributed to its much lower phase PM flux linkage. In addition, the proposed ASP machine has higher peak power maintain capability than the conventional counterpart due to its higher torque capability.

F. Mechanical Analyses

Since the proposed ASP-FRPM machine suffers from uncompensated radial forces since N_r is an odd number, the mechanical analyses of the FRPM machines with conventional and ASP structures should be carried out. The normal force and radial stress distributions of the two machines with 16 and 17 rotor poles under rated speed are shown in Figs. 20 and 21, respectively. In addition, the corresponding maximum electromagnetic force and stress results of the two investigated machines are tabulated in Table VI. Overall, the maximum normal forces and mechanical stresses of the ASP machine are much higher than those of the conventional one regardless of load currents. This is mainly due to the flux leakage suppression effect of the proposed ASP-FRPM machine, which experiences higher flux densities and thus more magnetic saturation in the stator core. Besides, it demonstrates that the maximum normal forces and stresses of the 17-rotor case are slightly higher than those of 16-rotor case for the ASP structures under the on-load operation. This is mainly due to the unbalanced magnetic pull of the 17-rotor FRMs. Nevertheless, it is worth mentioning all the stress results are much lower than the maximum allowed yield strength (435MPa), which permit the stable operation.

TABLE IV
COMPARISON OF LOSS CHARACTERISTICS OF 12/17-POLE FRPM MACHINES WITH CONVENTIONAL AND ASP CONFIGURATIONS @ RATED-LOAD, AND 1000 R/MIN

Items	Unit	Conventional	ASP
Iron loss (stator)	W	12.19	13.94
Iron loss (rotor)	W	5.70	5.30
Iron loss (eddy-current)	W	10.22	10.95
Iron loss (hysteresis)	W	7.67	8.29
Copper loss	W	143	139
Magnet loss	W	2.51	2.34
Output power	W	560	700
Efficiency	%	77.41	81.34

TABLE V
COMPARISON OF FLUX-WEAKENING CHARACTERISTICS OF 12/17-POLE FRPM MACHINES WITH CONVENTIONAL AND ASP CONFIGURATIONS
(U_{LIM}=120V, I_{LIM}=14.14A)

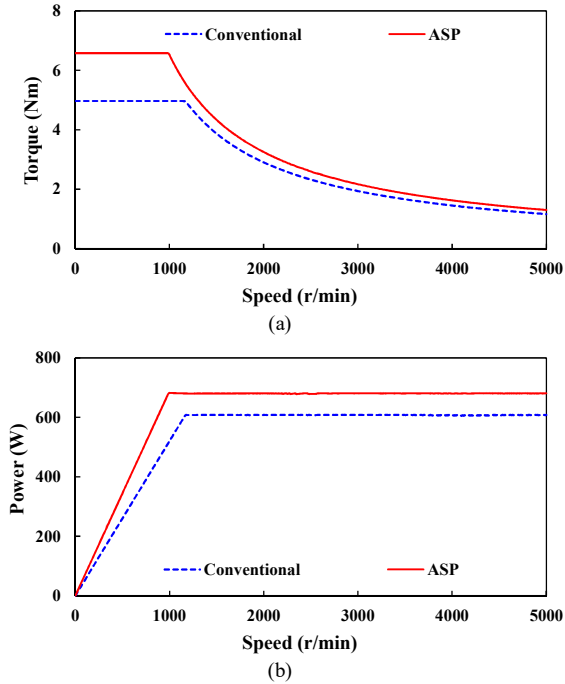| Items	Unit	Conventional	ASP
Base speed	r/min	1180	1000
Peak power	W	560	700
Phase flux linkage	mWb	14.95	21.13
d-axis inductance	mH	2.76	2.37
k_{fw}	-	1.84	1.12

Fig. 19. (a) Torque versus speed curves. (b) Power versus speed curves. (DC-link voltage=120V, peak current=14.14A)
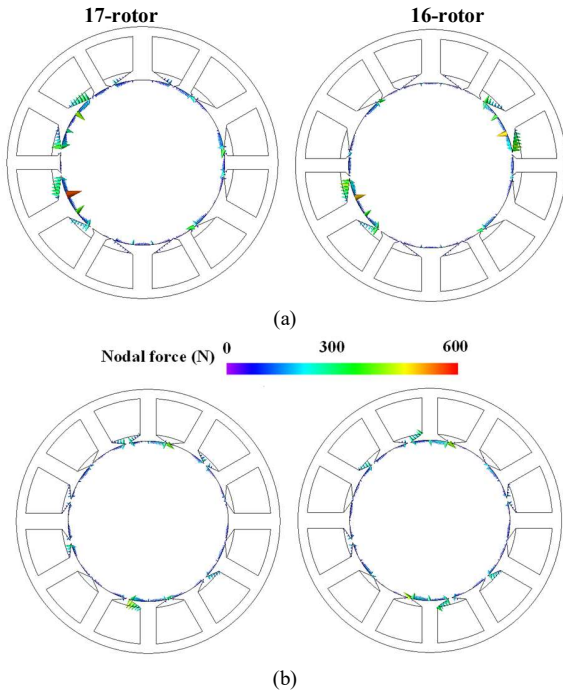

Fig. 20. FE-predicted normal force distributions of the conventional and ASP-FRPM machines @ rated load and speed. (a) ASP. (b) Conventional.

G. Remarks

Based on the foregoing electromagnetic performance comparison results, the merits and demerits of the proposed ASP-FRPM machine in relative to the conventional counterpart can be summarized as follows:

1) In terms of the advantages, the back-EMF magnitude and the average torque of the proposed ASP-FRPM machine are higher than those of the conventional FRPM machine, which is due to its flux leakage reduction effect. In addition, due to significantly higher torque capability, the ASP machine exhibits higher efficiency and higher peak power maintain capability than the conventional structure.

2) In terms of the disadvantages, the slightly higher cogging torque can be observed in the ASP structure. Due to the magnetic saturation caused by the biased flux linkage, the proposed ASP-FRPM machine shows non-linear torque-current feature, slightly higher iron loss and magnet loss, and comparable copper loss than the conventional case under rated load and speed. In addition, the maximum normal forces and stresses of the ASP machine are much higher than those of the conventional one.
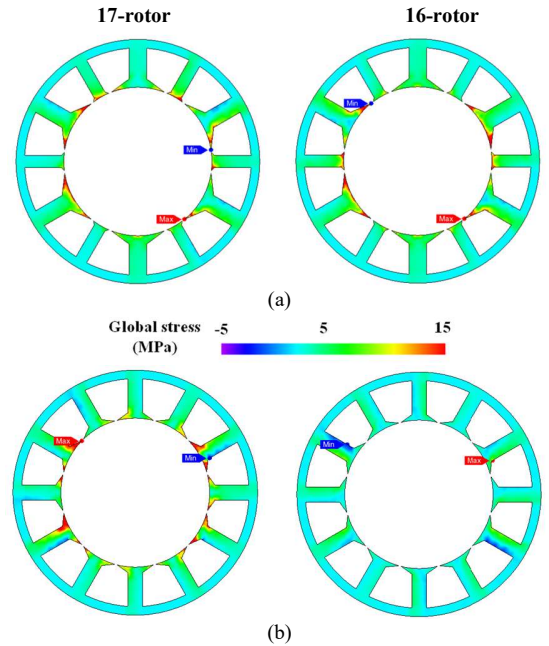

Fig. 21. FE-predicted radial stress distributions of the conventional and ASP-FRPM machines @ rated load and speed. (a) ASP. (b) Conventional.

TABLE VI
COMPARISON OF MAXIMUM ELECTROMAGNETIC FORCE AND STRESS RESULTS OF 16/17-ROTOR-POLE FRPM MACHINES WITH CONVENTIONAL AND ASP CONFIGURATIONS

Machine	Unit	No-load	Rated-load
Nodal force			
16-rotor Conventional	N	101.61	352.38
16-rotor ASP	N	206.52	490.20
17-rotor Conventional	N	130.57	391.56
17-rotor ASP	N	203.71	557.99
Radial stress			
16-rotor Conventional	MPa	2.42	4.80
16-rotor ASP	MPa	4.57	13.88
17-rotor Conventional	MPa	2.49	5.64
17-rotor ASP	MPa	4.57	13.99
Tangential stress			
16-rotor Conventional	MPa	3.62	24.98
16-rotor ASP	MPa	7.68	42.80
17-rotor Conventional	MPa	3.78	28.98
17-rotor ASP	MPa	8.26	46.80

VI. EXPERIMENTAL VALIDATION

In order to experimentally verify the above analyses, the optimized 12-stator-slot/17-rotor-pole ASP-FRPM machine prototype is manufactured and tested. The stator and rotor assemblies are shown in Fig. 22.
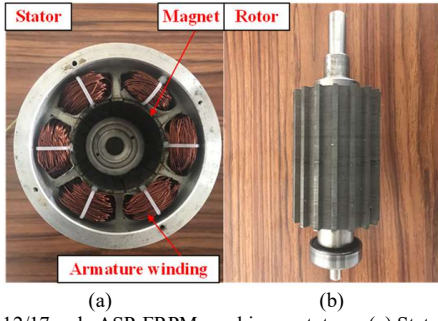
(a)   (b)

Fig. 22. The 12/17-pole ASP-FRPM machine prototype. (a) Stator. (b) Rotor.
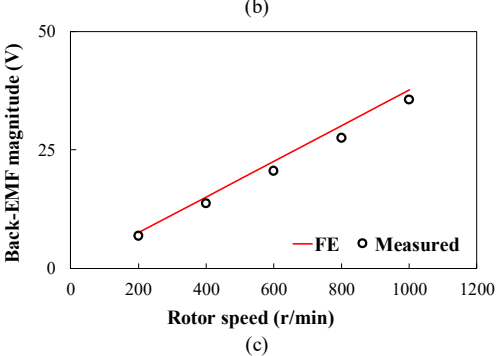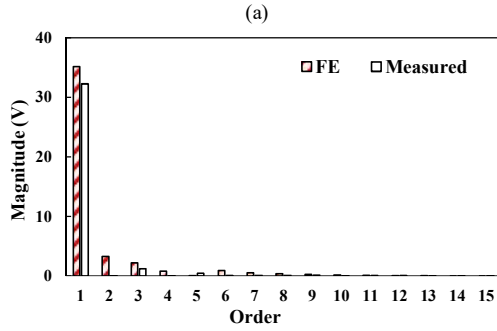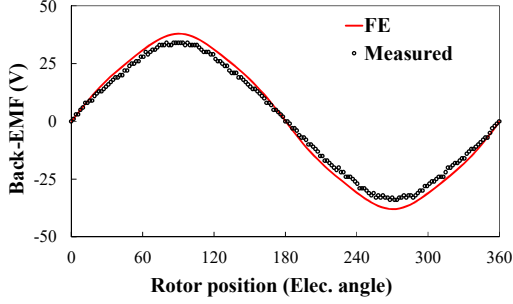

(a)

(b)

(c)

Fig. 23. Comparison of FE and measured back-EMFs of the prototype ASP-FRPM machine. (a) Waveforms. (b) Harmonic spectrum. (c) Fundamental EMF versus speed curve.

The open-circuit phase back-EMF, harmonic spectrum and the fundamental EMF versus speed curve for the prototype machine are measured and compared with FE-predicted results, as shown in Fig. 23. It can be seen that both the EMF waveforms show satisfactory sinusoidal levels, with low total harmonic distortions (THDs) of 5.64% and 4.95% for the FE and test results, respectively. Figs. 24 and 25 show the FE predicted and measured static torque versus speed, as well as torque against current characteristics. The slight difference between FE and measured results is mainly due to the fact that the end-effects and the mechanical tolerance are not considered

in the FE analyses. In addition, under the rated-load operation, the FE-predicted and measured loss/efficiency against rotating speed curves are shown in Figs. 26 and 27. The mismatch between the loss and efficiency results are mainly caused by the relative errors of the FE iron loss model and predicted mechanical loss. The abovementioned FE-predicted and measured results are quantitatively compared, as listed in Table VII. Overall, good agreement between FE predicted and test results confirms the aforementioned theoretical analyses.
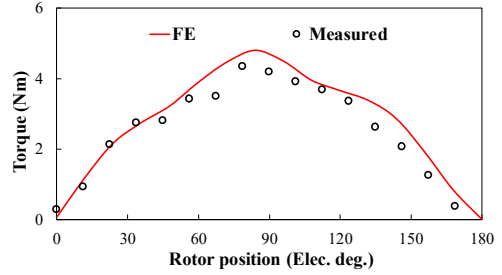

Fig. 24. Comparison of FE and measured static torque against rotor position curves. (I_a=-2I_b=-2I_c=10A)
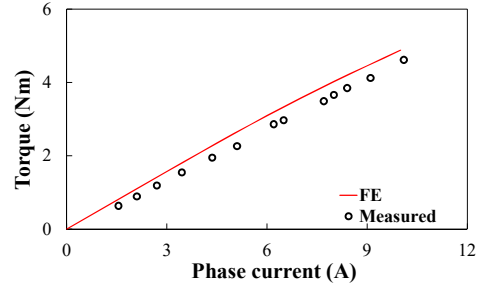

Fig. 25. Comparison of FE and measured torque against current curves.
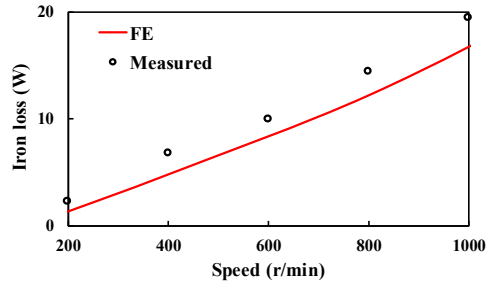

Fig. 26. Comparison of FE and measured iron loss against speed curves under rated load.
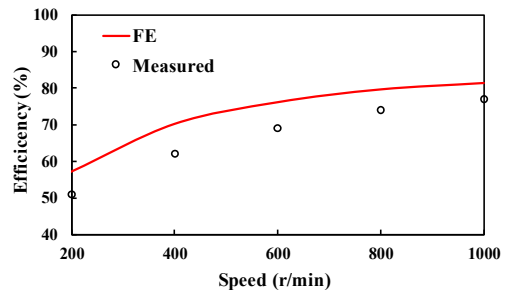

Fig. 27. Comparison of FE-predicted and measured efficiency against speed curves under rated load.

TABLE VII
COMPARISON OF FE-PREDICTED AND MEASURED OPEN-CIRCUIT EMF
CHARACTERISTICS, AND RATED-LOAD IRON LOSS, EFFICIENCY, AS WELL AS
POWER FACTOR @ 1000 R/MIN

Item	Unit	FE	Measured
Fundamental EMF	V	37.66	35.60
THD	%	5.64	4.95
Iron loss	W	16.72	19.45
Efficiency	%	81.41	77.60
Power factor	-	0.80	0.76

VII. CONCLUSIONS

This paper proposes a novel ASP-FRPM machine with asymmetric "NSN-S-NSN" PM arrangement. The flux leakage reduction mechanism is analytically investigated and confirmed, which indicates that the existence of biased coil flux linkage results in torque improvement of the proposed ASP design. The rotor pole number is analytically optimized with the aid of simplified permeance model. It can be found that the 12-stator-slot/17-rotor-pole configuration exhibits the highest torque capability. The design parameters are then globally optimized with the GA algorithm in order to improve the torque quality. Furthermore, the electromagnetic characteristics of the ASP- and conventional FRPM machines are analyzed and compared. It shows that the proposed ASP machine can provide 24.16% higher average torque, 30.04% lower torque ripple, 29% power factor improvement, as well as higher efficiency and peak power maintain capability than its conventional counterpart. In addition, the ASP structure shows higher iron loss and maximum normal forces and mechanical stresses than the conventional case. Finally, the satisfactory agreement between FE predicted and experimental results validates the theoretical analyses and the advantage of the proposed ASP design.

REFERENCES

[1] M. Cheng, W. Hua, J. Zhang, and W. Zhao, "Overview of stator permanent magnet brushless machines," *IEEE Trans. Ind. Electron.,* vol. 58, no. 11, pp. 5087-5101, Nov. 2011.

[2] X. Y. Ma, G. J. Li, G. W. Jewell, Z. Q. Zhu, and H. L. Zhan, "Performance comparison of doubly salient reluctance machine topologies supplied by sinewave currents," *IEEE Trans. Ind. Electron.*, vol. 63, no. 7, pp. 4086-4096, Oct. 2016.

[3] I. Boldea, L. N. Tutelea, L. Parsa, and D. Dorrell, "Automotive electric propulsion systems with reduced or no permanent magnets: an overview," *IEEE Trans. Ind. Electron.*, vol. 61, no. 10, pp. 5696-5711, Oct. 2014.

[4] T. Fukami, Y. Matsuura and K, Shima, "A multipole synchronous machine with non-overlapping concentrated armature and field windings on the stator," *IEEE Trans. Ind. Electron*., vol. 59, no. 6, pp. 2583-2591, Jun. 2012.

[5] Y. Liao, F. Liang, and T. A. Lipo, "A novel permanent magnet motor with doubly salient structure," *IEEE Trans. Ind. Appl.*, vol. 31, no. 5, pp. 1069-1078, Sep./Oct. 1995.

[6] D. Wu, J. T. Shi, Z. Q. Zhu, and X. Liu, "Electromagnetic performance of novel synchronous machines with permanent magnets in stator yoke," *IEEE Trans. Magn.*, vol. 50, no. 9, Art. No. 8102009, Sept. 2014.

[7] I. A. A. Afinowi, Z. Q. Zhu, Y. Guan, J. C. Mipo, and P. Farah, "A novel brushless ac doubly salient stator slot permanent magnet machine," *IEEE Trans. Energy Convers.*, vol. 31, no. 1, pp. 293-292, Mar. 2016.

[8] Y. Wang and Z. Deng, "Hybrid excitation topologies and control strategies of stator permanent magnet machines for DC power system," *IEEE Trans. Ind. Electron.*, vol. 59, no. 12, pp. 4601-4616, Dec. 2012.

[9] J. T. Chen and Z. Q. Zhu, "Winding configurations and optimal stator and rotor pole combination of flux-switching PM brushless AC machines," *IEEE Trans. Energy Convers.*, vol. 25, no. 2, pp. 293–302, Jun. 2010.

[10] R. P. Deodhar, S. Andersson, I. Boldea, and T. J. E. Miller, "The flux-reversal machine: a new brushless doubly-salient permanent magnet machine," *IEEE Tans. Ind. Appl.*, vol. 33, no. 4, pp. 925-934, Jun. /Aug. 1997.

[11] I. Boldea, L. Zhang, and S. A. Nasar, "Theoretical characterization of flux reversal machine in low-speed servo drives-the pole-PM configuration," *IEEE Trans. Ind. Appl.*, vol. 38, no. 6, pp. 1549–1557, Nov./Dec. 2002.

[12] C. H. T. Lee, K. T. Chau, and C. Liu, "Design and analysis of a cost-effective magnetless multiphase flux-reversal DC-field machine for wind power generation," *IEEE Trans. Energy Convers.*, vol. 30, no. 4, pp. 1565-1573, Jun. 2015.

[13] Y. Gao, R. Qu, D. Li, J. Li, and L. Wu, "Design of three-phase flux-reversal machines with fractional-slot windings" *IEEE Tran. Ind. Appl*, vol. 52, no. 4, pp. 2856-2864, Jul. 2016.

[14] D. More and B. Fernandes, "Power density improvement of three phase flux reversal machine with distributed winding," *IET J. Elect. Power Appl.*, vol. 4, no. 2, pp. 109–120, Feb. 2010.

[15] D. S. More, and B. G. Fernandes, "Analysis of flux-reversal machine based on fictitious electrical gear," *IEEE Trans. Energy Convers.*, vol. 25, no. 4, pp. 940-947, Dec. 2010.

[16] W. Zhao, J. Zheng, J. Wang, G. Liu, J. Zhao, and Z. Yang, "Design and analysis of a linear permanent-magnet vernier machine with improved force density," *IEEE Trans. Ind. Electron.*, vol. 63, no. 4, pp. 2072-2082, Apr. 2016.

[17] Y. Gao, R. Qu, D. Li, and G. Zhou, "Consequent-pole flux-reversal permanent-magnet machine for electric vehicle propulsion," *IEEE Trans. Appl. Supercond.*, vol. 26, no. 4, 5200105, Jun. 2016.

[18] H. Yang, H. Lin, Z. Q. Zhu, S. Fang, and Y. Huang, "A novel flux reversal hybrid magnet memory machine," in *Proc. Energy Convers. Congress and Expo. (ECCE)*, 2017 IEEE, Cincinnati, USA, 2017. 10.1-10.5.

[19] H. Yang, S. Lyu, H. Lin, and Z. Q. Zhu, "A variable-mode stator consequent pole memory machine," *AIP Advances*, vol. 8, no. 5, Art. No. 056612, 2018.

[20] D. Li, Y. Gao, R. Qu, J. Li, Y. Huo, H. Ding, "Design and analysis of a flux reversal machine with evenly distributed permanent magnets," *IEEE Trans. Ind. Appl.*, vol. 54, no. 1, pp. 172-183, Jan./Feb. 2018.

[21] H. Y. Li and Z. Q. Zhu, "Influence of magnet arrangement on performance of flux reversal permanent magnet machine," in *Proc. Int. Electr. Mach. Drives Conf. (IEMDC)*, May 2017, pp. 1–8.

[22] X. Zhu, W. Hua, W. Wang, and W, Huang, "Analysis of back-EMF in flux-reversal permanent magnet machines by air-gap field modulation theory," *IEEE Trans. Ind. Electron.,* in press.

[23] H. Y. Li, Y. Liu, and Z. Q. Zhu, "Comparative study of air-gap field modulation in flux reversal and vernier permanent magnet machines," *IEEE Tran. Magn.*, in press.

[24] X. Zhu and W. Hua, "An improved configuration for cogging torque reduction in flux-reversal permanent magnet machines," *IEEE Tran. Magn.*, vol. 53, no. 6, 8102504, Jun. 2017.

[25] Y. Kim, T. Kim, Y. Kim, W. Oh, and J. Lee, "Various design techniques to reduce cogging torque in flux-reversal machines," in *Proc. of Int. Conf. Elect. Mach. & Syst.*, Nanjing, China, Oct. 2005, pp. 261-263.

[26] G. Vakil, P. Upadhyay, N. Sheth, A. Patel, A. Tiwari, and D. Miller, "Torque ripple reduction in the flux reversal motor by rotor pole shaping and stator excitation," in *Proc. of Int. Conf. Elect. Mach. & Syst.*, Wuhan, China, Oct. 2008, pp. 2980-2985.

[27] G. Qi, J. T. Chen, Z. Q. Zhu, D. Howe, L. B. Zhou, and C. L. Gu, "Influence of skew and cross-coupling on flux-weakening performance of permanent magnet brushless AC machines," *IEEE Trans. Magn.*, vol. 45, no. 5, pp. 2110–2117, May 2009.

[28] Z. Q. Zhu and X. Liu, "Individual and global optimization of switched flux permanent magnet motors," in *Proc. Int. Conf. Electr. Machin. Syst.*, (*ICEMS 2011*), Aug. 2018, pp. 1-6.

[29] Q. Lu, Y. Yao, J. Shi, Y. Shen, X. Huang, and Y. Fang, "Design and performance investigation of novel linear switched flux PM machines," *IEEE Trans. Ind. Appl.*, vol. 53, no. 5, pp. 4590-4602, Sept./Oct. 2017.

[30] Z. Q. Zhu, Z. Z. Wu, and X. Liu, "A partitioned stator variable flux reluctance machine," *IEEE Trans. Energy Convers.*, vol. 31, no. 1, pp. 78-92, Mar. 2017.